Beating of Aharonov-Bohm oscillations in a closed-loop interferometer

Sanghyun Jo,[1,2] Gyong Luck Khym,[3] Dong-In Chang,[1,2] Yunchul Chung,[4,*] Hu-Jong Lee,[1,2,†] Kicheon Kang,[3] Diana Mahalu,[5] and Vladimir Umansky[5]

[1]*Department of Physics, Pohang University of Science and Technology, Pohang 790-784, Republic of Korea*
[2]*National Center for Nanomaterials Technology, Pohang 790-784, Republic of Korea*
[3]*Department of Physics and Institute for Condensed Matter Theory, Chonnam National University, Gwangju 500-757, Republic of Korea*
[4]*Department of Physics, Pusan National University, Busan 609-735, Republic of Korea*
[5]*Department of Condensed Matter Physics, Weizmann Institute of Science, Rehovot 76100, Israel*

One of the points at issue with closed-loop-type interferometers is beating in the Aharonov-Bohm (AB) oscillations. Recent observations suggest the possibility that the beating results from the Berry-phase pickup by the conducting electrons in materials with the strong spin-orbit interaction (SOI). In this study, we also observed beats in the AB oscillations in a gate-defined closed-loop interferometer fabricated on a GaAs/Al$_{0.3}$Ga$_{0.7}$As two-dimensional electron-gas heterostructure. Since this heterostructure has very small SOI, the picture of the Berry-phase pickup is ruled out. The observation of beats in this study, with the controllability of forming a single transverse subband mode in both arms of our gate-defined interferometer, also rules out the often-claimed multiple transverse subband effect. It is observed that nodes of the beats with an $h/2e$ period exhibit a parabolic distribution for varying the side gate. These results are shown to be well interpreted, without resorting to the SOI effect, by the existence of two-dimensional multiple longitudinal modes in a single transverse subband. The Fourier spectrum of measured conductance, despite showing multiple h/e peaks with the magnetic-field dependence that are very similar to that from strong-SOI materials, can also be interpreted as the two-dimensional multiple-longitudinal-modes effect.

I. INTRODUCTION

An electron traversing a path enclosing magnetic flux acquires an additional phase by the magnetic vector potential. This additional phase causes the Aharonov-Bohm (AB) oscillation of the electronic magnetoconductance[1] with the period of h/e. The AB oscillation in solid state devices was first observed by Webb *et al.*[2] and Timp *et al.*[3] in metal and semiconductor AB rings, respectively. Especially, AB rings fabricated on the two-dimensional electron-gas (2DEG) layer formed in a semiconductor heterojunction structure such as GaAs/AlGaAs have been studied intensively, because the electron phase coherence in this system extends much longer than the size of an AB ring.

For instance, a structure of a quantum dot embedded in one arm of an AB ring was employed recently for accurate measurements of the phase change of traversing electrons through a quantum dot. Yacoby *et al.*[4] first demonstrated that the electron transport through a quantum dot embedded in a closed-loop AB interferometer was phase coherent. However, the phase rigidity, imposed by the Onsager relation in the two-terminal geometry of an AB ring, hampered measurements of the genuine phase variation through the quantum dot.[5] Later on, Schuster *et al.*[6] measured the phase evolution via a resonant level of a quantum dot embedded in an open-loop AB interferometer, which allowed multiterminal conductance measurements while breaking the time-reversal symmetry of the system. Many other phase measurements through various quantum structures were followed by using the open-loop AB interferometer.[7] Although open-loop AB interferometers are more useful for measuring the phase of

the embedded quantum structures, closed-loop AB interferometers are still in often use because of a simpler theoretical interpretation of the results.

Detailed studies on closed-loop interferometers, however, often revealed beats in its AB magnetoconductance oscillation.[8,10] Beats were first explained in terms of mixing of different multiple transverse subband modes arising from a finite width of a ring.[8] The transverse subband modes, with the conductance of $2e^2/h$ per mode, are the quantum states defined by the transverse potential in the interferometer, which can be tuned by the voltages applied to the gates, i.e., quantum point contacts. This model, however, failed to explain the appearance of beats in the conductance with a single transverse subband (STSB) mode, which was observed by the same group.[8] Later, Tan and Inkson[9] pointed out that the clockwise and the counterclockwise moving electron states in an STSB mode may generate different AB-oscillation frequencies, producing the beats reported in Refs. 8 and 10. In the meantime, similar beating effect was observed in the AB interferometry using 2DEG [two-dimensional hole gas (2DHG)] systems based on strong spin-orbit interaction (SOI) materials such as InAs and InGaAs [GaAs] heterojunctions.[11–14] It was interpreted as the evidence for the revelation of the Berry phase[15] caused by the strong SOI. In this case, the Fourier spectrum of the beat pattern showed multiple splitting of the h/e peak. Morpurgo *et al.*[11] and Meijer *et al.*[12] showed clear splitting of the h/e peak into multiple peaks in the ensemble-averaged Fourier spectrum over several measurements for a fixed and varied gate voltage(s), respectively. They attributed the splitting to the Berry-phase[15] pickup by the traversing electrons due to the SOI. Yau *et al.*[13] and Yang *et al.*[14] also observed the

multiple splitting of a single Fourier-spectrum peak and the evolution of the spectrum for varying magnetic fields. Based on the numerical simulation, the authors also attributed them to the result of the Berry-phase pickup. All these works, however, did not consider the effect of possible mixing of multiple conducting channels.

In this study, we investigated the behavior of the magnetoconductance from a closed-loop AB interferometer fabricated on a GaAs/Al$_{0.3}$Ga$_{0.7}$As heterostructure 2DEG, with a very weak SOI. The magnetoconductance always revealed clear beats of AB oscillations. The corresponding Fourier spectrum exhibited multiple peaks closely spaced around the field value where the h/e peak was expected. The patterns were very similar to those observed previously from the AB rings fabricated on strong-SOI materials. To interpret our observation of the beats in our system with a very weak SOI, we simulated two-dimensional (2D) AB ring using the method adopted by Tan and Inkson.[9] In the simulation, even in a fixed transverse subband mode, additional eigenmodes existed to contribute to the electron transport as a function of the Fermi level and a magnetic field. For the remainder of this paper, these modes will be referred as longitudinal modes. These modes were found to evolve in different ways depending on the geometry and thus induce beats of AB oscillations in a 2D interferometer. We were able to explain all our results in terms of the formation of the 2D multiple longitudinal modes in an STSB without resorting to the strong-SOI effect. In fact, measurements of the weak localization (WL) and the Shubnikov–de Haas (SdH) oscillation in our system revealed that the SOI was almost negligible. In our observation, the $h/2e$ periodicity was noticeable only around the nodes of the beats. In addition, the nodes of the beats formed a parabolic distribution for varied voltages applied to one of the loop-forming side gates, which was not observed in the previous studies.[8–10] These two general features of our data were in accordance with the prediction of the 2D multiple-longitudinal-modes effect in an STSB.

II. RESULTS AND DISCUSSION

A. Device structure and measurements

Figure 1 shows a gate-defined closed-loop AB interferometer, fabricated on a wafer of GaAs/Al$_{0.3}$Ga$_{0.7}$As heterostructure 2DEG. The electron density of the 2DEG was about 2 $\times 10^{11}$ cm^{-2} with the mobilities higher than 2 $\times 10^{6}$ cm^2 V^{-1} s^{-1} at 4.2 K. The 2DEG layer resided 70 nm below the surface of the wafer. The interferometer was defined by an island gate, four side gates, and two quantum-dot gates as shown in the figure. The shape of this structure is similar to the one reported previously.[4] The electron path inside the interferometer was defined by tuning negative voltages to these gates. Unlike a closed-loop interferometer defined by the mesa formation,[8,10–14] the number of transverse conducting channels (subbands) in each (left or right) arm could be fine tuned by the six side gates. This was a big advantage over mesa-defined AB rings, where the existence of multiple transverse subbands was inevitable in practice. In our study, the number of transverse subbands for each path was kept close to or below 1 to avoid any possible interfer-
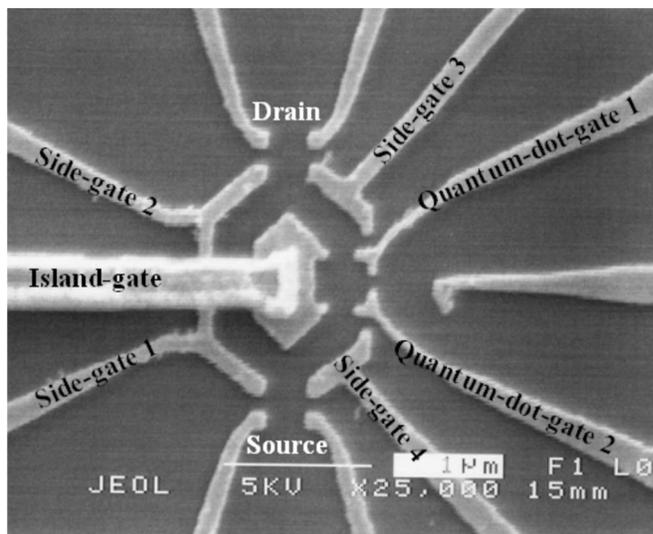

FIG. 1. SEM image of the gate-defined closed-loop Aharonov-Bohm interferometer fabricated on a GaAs/Al$_{0.3}$Ga$_{0.7}$As heterostructure two-dimensional electron-gas layer.

ence among electrons from different transverse subbands. The quantum dot embedded in the interferometer in Fig. 1 was not formed during measurements of beats, despite the physical presence of the gates to form it in the sample. All the measurements were made at the base temperature of 10 mK in a dilution fridge. The corresponding electron temperature estimated from measurements of the Coulomb blockade in the quantum dot[16] was around 140 mK. The standard phase-sensitive lock-in technique was employed to improve the signal to noise ratio. The AB magnetoconductance oscillations were taken by observing the current between the two ends (the source and the drain) of the AB ring in an excitation voltage of 10 μV rms. For measurements of the WL and the SdH oscillation, a four-probe configuration was employed, where a 15 nA rms current was applied between the source and the drain while monitoring the corresponding voltage difference.

B. Gate-voltage dependence of beats

The magnetoconductance of the interferometer at various voltages of side gate 1 (V_{sg1}) was measured by applying a 10 μV rms excitation voltage to the interferometer while monitoring the source-drain current. The magnetic field was swept in the range between -1500 and 1500 G, while the V_{sg1} was varied from -271.35 to -291.15 mV at intervals of 1.65 mV. Since the conductance for any V_{sg1} was lower than $2e^2/h$, it was assumed that less than an STSB[28] was open for each path of the interferometer. Since the visibility of the AB oscillation was about 2%, the background current level was subtracted for clarity. As shown in Fig. 2(a), the field dependence of the conductance exhibits clear beats of AB oscillations for any values of V_{sg1}. In addition, the phase evolved discontinuously in the variation range of V_{sg1}. This phenomenon of the rigid phase has been observed by others[4,17] and interpreted by the Onsager relation in a two-terminal closed-loop interferometer.[5] The relation stipulates that the elec-
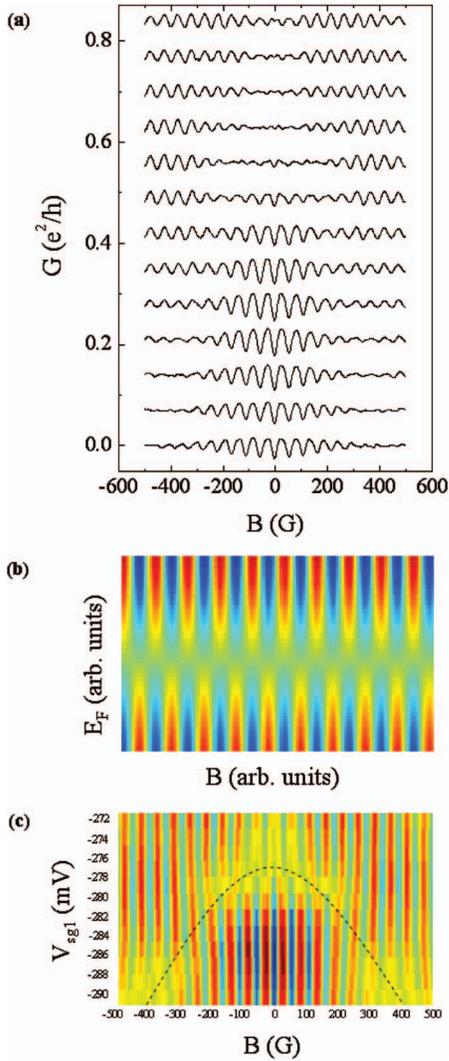
FIG. 2. (Color) (a) The magnetoconductances for various voltage to side gate 1, V_{sg1}, after subtracting the smooth backgrounds from the raw data, as a function of magnetic fields. The magnetic field was varied from −500 to 500 G, while V_{sg1} from −271.35 mV (top) to −291.15 mV (bottom) at intervals of 1.65 mV. (b) The phase rigidity expected in a one-dimensional closed-loop AB ring is illustrated. (c) The two-dimensional pseudocolor plot of the magnetoconductance shown in (a). A double-frequency regime is guided by the dashed line. For both pseudocolor plots, the red (blue) color represents the high (low) magnetoconductance.

tronic conductance through a closed-loop interferometer should be symmetric with respect to the $B=0$ axis, allowing only 0 or π phase. As a result, the phase change occurs only by π via a double-frequency ($h/2e$ period) AB-oscillation regime.[4,5] The expected phase change in a one-dimensional (1D) closed-loop interferometer, with an STSB per path without considering finite width of the electron path, is shown in Fig. 2(b). As in the figure, the phase stays unaltered for the variation of the Fermi energy (E_F) in the leads until it suddenly changes by π. The simulation also suggests that the frequency of the AB oscillation doubles with $h/2e$ periodicity between the transition of the two phase states. For a 1D closed-loop interferometer, with an STSB in each arm, this

transition should occur at the same E_F in all magnetic fields. In other words, as in Fig. 2(b), the transition region should be parallel with the B-field axis. In our measurements, however, the transition region distributes rather parabolically in the V_{sg1}-vs-B-field plot [Fig. 2(c)]. These features were reproducible even after thermal recycling. References 10 and 14 report the existence of $h/2e$ period in the beats of AB oscillations, but without this parabolic distribution. Similar behavior was observed with the variation of the source-drain bias voltage. A parabolic distribution of the transition regions was also observed when the voltage of the island gate was varied while fixing the voltages for all the other gates used to form the interferometer.

C. Strength of the spin-orbit interaction in GaAs/Al$_{0.3}$Ga$_{0.7}$As heterostructure

Such a beating effect without the parabolic distribution of the $h/2e$ transition region mentioned above has been observed in various systems such as metallic AB rings,[2,18] GaAs/AlGaAs 2DEG AB rings,[8,10] GaAs/AlGaAs 2DHG rings,[13] and InAs-based[11,14] and InGaAs-based[12] 2DEG rings. Although the beating features are similar to each other, interpretations of the origin of the beats are varied. Two main models suggested to explain the beats are based on picking up the Berry phase induced by the SOI and mixing of multiple conducting channels caused by the finite width of an AB ring involved. The Berry-phase-related interpretation of the beats is favored for the AB rings formed on the relatively strong SOI systems such as GaAs/AlGaAs-based 2DHG and InAs-based and InGaAs-based 2DEG's. In contrast, the model of mixed multiple conducting channels is favored for AB rings in metallic films and GaAs/AlGaAs-based 2DEG's with relatively small SOI.[19]

To estimate the strength of the SOI in our system, both the WL and the SdH oscillation were measured on an identical sample that was used to measure the beats. Fitting the antilocalization dip in the magnetoresistance for strong-SOI materials leads to resolving the SOI strength.[20] By contrast, the SOI gives two different frequencies for the SdH oscillation. It results in beats in the SdH oscillation, allowing one to estimate the SOI strength.[21] Figures 3(a) and 3(b) illustrate the magnetoresistances of the WL and the SdH oscillation, respectively, measured in a Hall-bar geometry formed on our sample. All the gates in the interferometer were grounded during the measurements. Figure 3(a) shows the magnetoresistance averaged over 37 measurements with the field resolution of 0.2 G, which exhibits no discernible antilocalization dips. Figure 3(b) shows the measured SdH oscillation, without any beats either. These results strongly imply that the SOI was very weak or almost negligible in the GaAs/Al$_{0.3}$Ga$_{0.7}$As heterostructure 2DEG of our interferometer. Although it is known that metallic gates may enhance the strength of the SOI, the enhancement is usually less than 30% of the original value.[22] We thus expect that the SOI caused little effect on our magnetoconductance measurements.

D. Two-dimensional multiple-longitudinal-modes effect

In our measurements, only an STSB was set to open in each arm. The beats of AB oscillation for the STSB conduc-
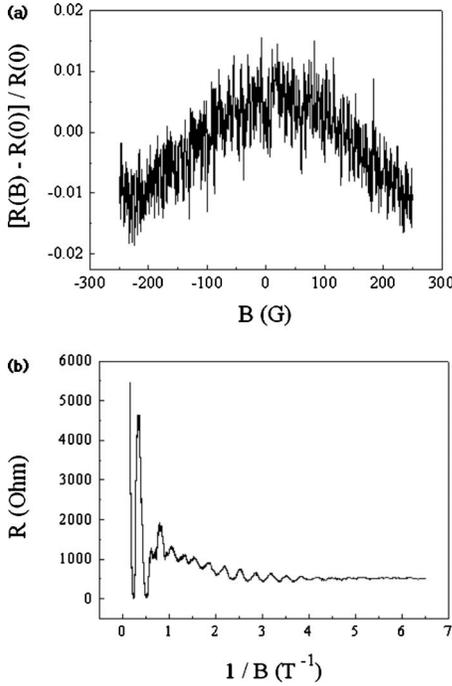
FIG. 3. (a) Normalized magnetoresistance averaged over 37 independent measurements and (b) the longitudinal Hall resistance of a Hall-bar structure, both plotted as a function of magnetic fields.

FIG. 4. (Color online) (a) The calculated energy-band diagram of a two-dimensional AB ring. The energy eigenvalues for $n=0$ and $|m| \leqslant 30$ modes are plotted as a function of magnetic fields. Multiple bands correspond to different m values. The filled circles denote the band-crossing points, while the open circles denote the middle point between two neighboring band-crossing points. (b) The band diagram of the dashed-box region in (a) enlarged for clarity.

tion were experimentally observed previously,[8,10] where the beats were theoretically interpreted in terms of mixing of clockwise and counterclockwise moving states of electrons with different frequencies[9] in an STSB mode. We employed the model as used in Ref. 9 to simulate the beats and the evolution of their transition region as a function of V_{sg1}. The result indicates that the multiple longitudinal modes existing in an STSB mode generate the AB oscillations. However, the multiple longitudinal modes give more than two oscillation frequencies, with the number of the oscillation frequencies varying with the magnetic field, due to the finite width of the electron path inside the interferometer. The magnetic-field dependence will be discussed in the next section in more detail.

We adopted the same form of the Shrödinger equation as used in Ref. 9, but with varied parameter values to fit our experimental conditions. The eigenvalues are

$$E_{n,m}(B) = \left(n + \frac{1}{2} + \frac{1}{2}\sqrt{m^2 + \frac{\eta^2}{4}} \right)\hbar\omega + \frac{m}{2}\hbar\omega_c - \frac{\eta}{4}\hbar\omega_0,$$

$$n = 0, 1, 2, 3, \ldots, \quad m = \ldots, -1, 0, 1, \ldots, \quad (1)$$

where $\omega_c = eB/\mu$, $\omega = \sqrt{\omega_c{}^2 + \omega_0{}^2}$, $\eta = \mu\omega_0 r_0{}^2/\hbar$, μ is the effective mass of the electron, ω_0 is the transverse confinement strength of the gates defining the electron path, and r_0 is the average radius of the interferometer. Here, the quantum number n is the transverse subband index and m is related with the longitudinal motion.[9] In our measurements, we tuned the interferometer to have an STSB, corresponding to $n=0$. In Fig. 4(a), the energy band $E_{n,m}(B)$ is shown for an STSB mode with $n=0$ and $|m| \leqslant 30$.
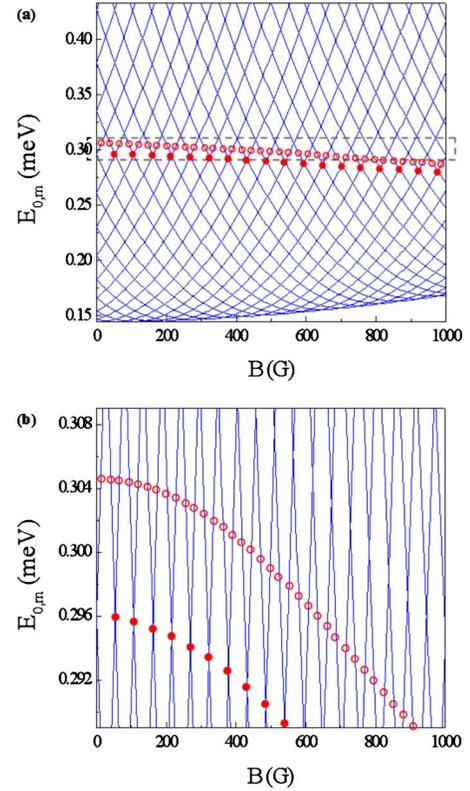
As shown in Fig. 4(a), several conducting modes exist even for an STSB mode because of the existence of multiple longitudinal modes. The corresponding energy eigenvalues depend on m as well as n. For this dependence, the dispersion of the bands is asymmetric about the band minima. The minima shift to higher energies for nonzero magnetic fields,[9] which results in breaking of the discrete symmetry under the translation along B axis. As indicated by filled (open) circles in the figure, this makes band-crossing (splitting) points respond nonlinearly to the applied magnetic field. Figure 4(b) is an expanded band diagram of the region in the dashed box in Fig. 4(a). The band-splitting points show a clear downturn curvature as represented by open circles, the shape of which is very similar to that of the conductance with the $h/2e$ period in Fig. 2(c).

The conductance for a given Fermi energy E_F in the dashed-box region in Fig. 4(a) was calculated using the Landauer-Büttiker formula[23]

$$G(E_F, B) = \frac{2e^2}{h} \sum_{n,m} \frac{\Gamma^2}{[E_F - E_{n,m}(B)]^2 + \Gamma^2}, \quad (2)$$

where only $n=0$ is taken into account and the transmission probability via an eigenmode is given by the Breit-Wigner formula at zero temperature. Here, Γ is the coupling constant
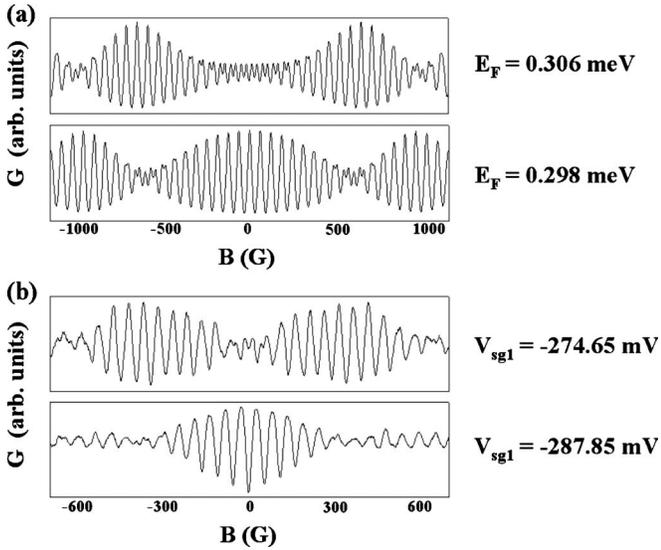
FIG. 5. (a) The magnetoconductance calculated for $E_F=0.306$ and 0.298 meV, where the Fermi energies were set to lie in the lowest subband to simulate the measurement condition. (b) Measured magnetoconductance for $V_{sg1}=-274.65$ and -287.85 mV.

between the emitter (or the collector) and the AB ring. The Γ was set at 3% of $\hbar\omega_0$, which corresponds to a weak coupling regime of the system. The calculated results are shown in Fig. 5(a). The conductance shows a clear beat pattern with a variation of the envelope as a function of E_F. Figure 5(b) shows similar behavior observed experimentally for varied V_{sg1}. The figures indicate that the $h/2e$ (h/e) oscillation predominates in the nodes (antinodes) of the beats. The region of dominant $h/2e$ oscillation appears in different magnetic fields as E_F is varied. A grayscale plot of the calculated conductance is shown in Fig. 6. The E_F was set to the range in the dashed square box in Fig. 4(a). The band shown in Fig. 4(b) is overlapped on the grayscale plot by white solid lines. Contrary to the results calculated for an STSB in a 1D interferometer as in Fig. 2(b), the region where the nodes of the beats appear shows an $h/2e$ oscillation and distributes para-
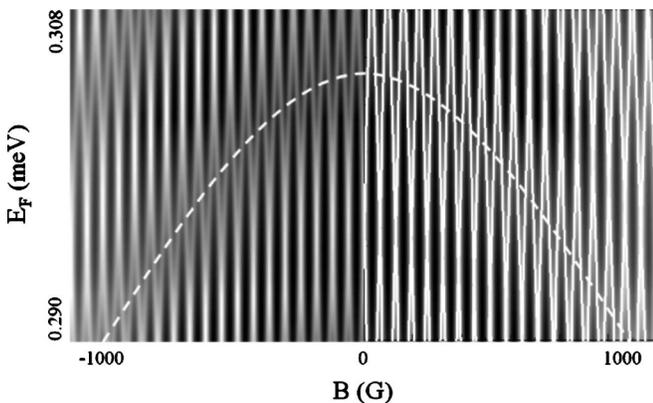

FIG. 6. Grayscale plot of the conductance, calculated for a two-dimensional electron-gas AB ring, as a function of E_F and magnetic field, where the band shown in Fig. 4(b) is overlapped in white solid lines. The white dashed line is a guide to denote the region where the $h/2e$ oscillation is dominant.

bolically in an E_F-vs-B-field plot. This result is in qualitative agreement with our observation shown in Fig. 2(c). Clearer revelation of the double-frequency region in the simulation may be from smaller Γ value and higher visibility of AB oscillations than those in the measurement. The parabolic evolution of the node region can be naively understood with the band diagram shown in Fig. 4. According to Eq. (2), the overall conductance through an AB ring is determined mainly by the bands located close to E_F. Hence, if E_F is at a crossing point of two bands (marked by a filled circle in the figure), the h/e oscillation becomes predominant. By contrast, the $h/2e$ oscillation predominates if E_F is at a band-splitting point marked by an open circle in the figure. The conductance itself is bigger for h/e oscillation, since two longitudinal modes simultaneously contribute to the conductance, while a single longitudinal mode contributes to the conductance for $h/2e$ oscillation. This is the reason why h/e ($h/2e$) oscillation is dominant in the antinodes (nodes). Since these band-crossing (splitting) points evolve parabolically as a function of E_F and B, the antinodes (nodes) also evolve in the same fashion. It should be emphasized that the finite width of the electron path in an AB interferometer is responsible for the parabolic evolution of the band-crossing points. According to our simulation, however, a parabolic evolution with an upturn curvature is also possible in different regions of E_F (not shown). Similar experimental result was also observed in a different region of the gate voltages.

The beat feature similar to Fig. 5 was reported in mesa-defined closed-loop AB interferometers,[8,10] with the results interpreted in terms of 2D multiple-longitudinal-modes effect[9] in an STSB. In these works, however, no parabolic evolution of the beat pattern was reported. The parabolic evolution gives an additional confirmation of the validity of the model and better understanding of the 2D multiple-longitudinal-modes effect in an STSB. Observing the smooth evolution of the node region was possible in our study, because the number of transverse subbands was fine controlled by the six individual gates, rather than by a single gate covering the whole mesa-defined AB ring as used in the other measurements. We tuned all the gates individually to leave an STSB open. Only one gate was then slightly modified to observe such an evolution.

E. Fourier-transform analysis and comparison with results from an Aharonov-Bohm ring of strong spin-orbit interaction

The Fourier-transform analysis is a very effective way to analyze the beating of AB oscillation induced both by the multiple-conducting-channel effect[8,10] and the SOI effect.[11–14] The Fourier spectrum gives the information on different conducting channels (or modes) inside an interferometer with very small frequency differences. In this section, we present the Fourier spectrum of two representative beats, which show the antinodes and the nodes at $B=0$. The zero-padding technique[24] that was used to analyze the beats induced by the SOI effect[13,14] was adopted for our Fourier transform analysis. The magnetoconductance data taken in the range between -1500 and 1500 G were used for the
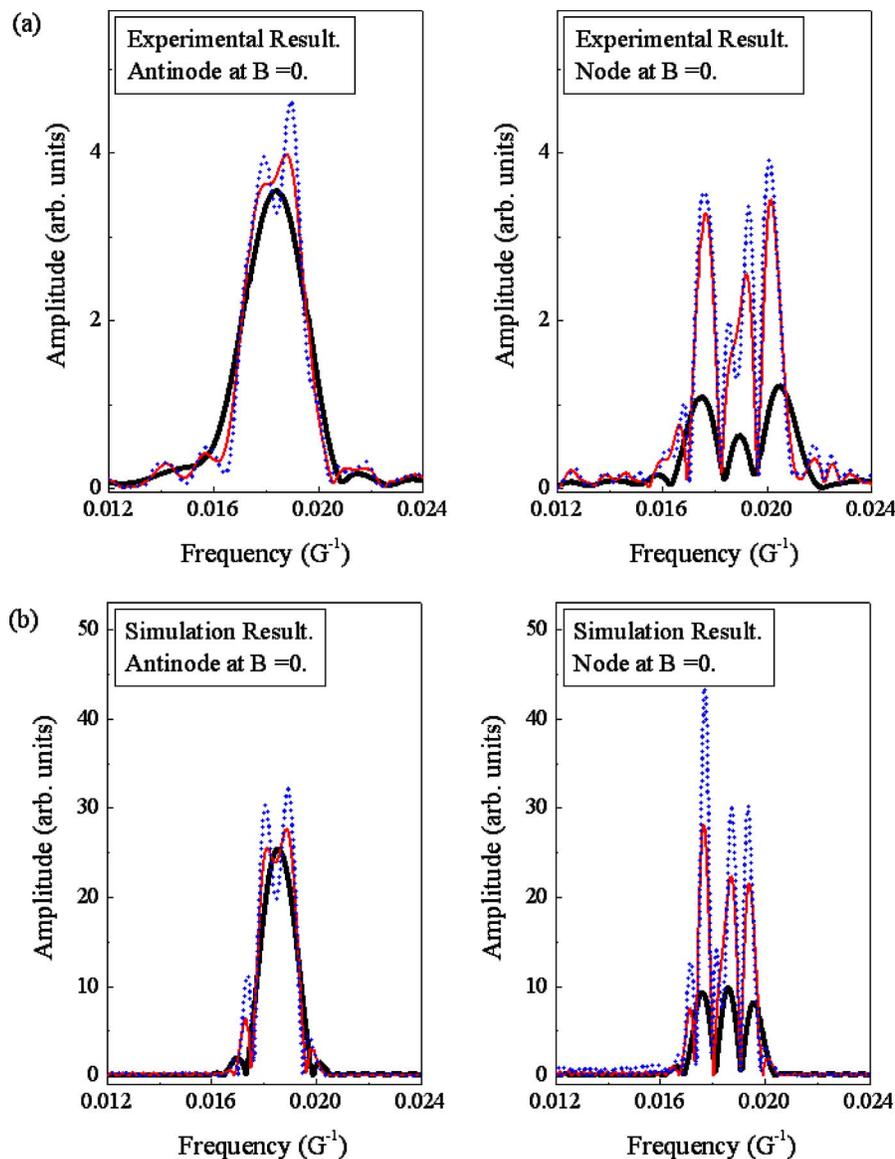
FIG. 7. (Color online) (a) The Fourier spectrum of the h/e magnetoconductance measured at different V_{sg1} in a few magnetic-field windows. In the left (right) panel, with $V_{sg1}=-289.50$mV $(-277.95$ mV), the antinode (node) of beats was at $B=0$. In the left (right) panel, the magnetic field was varied in the ranges of ±500 G $(\pm500$ G), ±900 G $(\pm1200$ G), and ±1200 G $(\pm1500$ G), indicated by the thick solid line, the thin solid line, and the dotted line, respectively. (b) The Fourier spectrum of h/e magnetoconductance calculated for different values of E_F and a few magnetic-field windows are shown for comparison. In the left (right) panel, with $E_F=0.297$ meV (0.305 meV), the beating features for $B=0$ are similar to those of (a). In the left (right) panel, the magnetic field was varied in the ranges of ±800 G $(\pm800$ G), ±1200 G $(\pm1600$ G), and ±1600 G $(\pm2400$ G), indicated by the thick solid line, the thin solid line, and the dotted line, respectively.

analysis, because SdH oscillation started to appear at around ±2000 G due to the high mobility of electrons in the sample. Within this range, four different widths of the Hamming window[25] (±500, ±900, ±1200, and ±1500 G) were used. This allowed a close examination of any field-dependent effect.

The left (right) panel of Fig. 7(a) is the Fourier spectrum for the antinode (node) at $B=0$. These two cases show different features, but their magnetic-field dependencies are similar to each other. When the antinode is at $B=0$, the Fourier spectrum shows a main center peak and a trace of small side peaks in a low-magnetic-field range. With increasing magnetic field, the main center peak starts to split, while the side peaks become clearer. When the node is at $B=0$, however, the amplitudes of the main center peak and symmetric side peaks are comparable even in a low-magnetic-field range. With increasing magnetic field in this case, the center peak starts to split, while the amplitudes of the side peaks increase. Figure 7(b) is the Fourier spectrum of the calculated magnetoconductance when an antinode and a node are

at $B=0$. The features are similar to those of the experimental Fourier spectrum.

The evolution of the Fourier spectrum as a function of the magnetic field can be naively explained as follows. First, the band-crossing points marked by filled circles in Fig. 4(a) give a Fourier-transform peak (the center peak). Second, open circles marked in the figure give two Fourier-transform peaks (the side peaks), where one is slightly lower and another is slightly higher than the peak given by the band-crossing points. These are major three peaks shown in the spectrum. The frequency difference and the field dependence of the peaks are caused by the breaking of the discrete symmetry under the translation along the B axis. Even with many energy bands around E_F, the conductance is mainly determined by the bands close to E_F. Thus, if the data showing an antinode at $B=0$ are taken for the Fourier-spectrum analysis with a very narrow magnetic-field window, only a center peak appears in the spectrum. As the width of the magnetic-field window increases, the nodal part is included in the analysis to produce the side peaks in the spectrum. By the

same analogy, if the data showing node at $B=0$ are taken for the analysis with a narrow magnetic-field window, only the side peaks appear in the spectrum. As the antinodal part is included in the analysis by enlarging the magnetic-field window, the center peak appears in the spectrum. These features are illustrated in Fig. 7(a). However, the experimental data given in the right panel of Fig. 7(a) show three peaks (a center peak and two side peaks) even in a low-magnetic-field range. That is because the magnetic-field window is wide enough to contain the antinodes as well as the node as shown in Fig. 2(a).

Similar evolution of Fourier-spectrum peaks as a function of magnetic field was also reported in Refs. 13 and 14. Those were interpreted as evidences for the Berry-phase pickup by the SOI, although the interpretation in Ref. 13 has been controversial.[26,27] We believe that the evolution of peaks observed in the Fourier spectrum as a function of magnetic fields is not a conclusive evidence of the spin-orbit coupling,[14] since the same effect is also observable in systems with negligible spin-orbit coupling. The beats in this case can be explained by the 2D effects inside the interferometer, as clearly demonstrated in our study, both in experiment and in simulation. Meanwhile, the center-peak splitting and the side peaks were also observed in other magnetoconductance measurements using AB rings fabricated on strong-SOI materials.[11,12] In these works, the splitting of the center peak was focused and regarded as an evidence for the Berry-phase pickup by the SOI. It was pointed out, however, that the splitting was too large to be explained by the Berry-phase pickup only. In those works, the existence of the side peaks was not clearly explained either. As shown in our data, the splitting of the center peaks in Fig. 7(a) is around 0.001 G^{-1}, which is comparable to those in Refs. 11 and 12. Even with almost negligible SOI in our system, the features of the Fourier spectrum of the measured magnetoconductance show a similarity to those found in strong-SOI systems.[11–14] Our study demonstrates that the features in the Fourier spectrum can be generated irrespective of the Berry-phase pickup.

III. SUMMARY AND CONCLUSION

The beats of AB oscillations in a closed-loop interferometer fabricated on GaAs/Al$_{0.3}$Ga$_{0.7}$As 2DEG were observed. Unlike mesa-defined interferometers, in our measurements, the electron path in each arm of the interferometer was kept less than a single transverse subband (STSB) by the fine control of six individual path-forming side gates. This enabled us to study the effect of the two-dimensional longitudinal modes developing in an STSB induced by the external magnetic field. Our simulation indicates that the experimentally observed beats of AB oscillations resulted from the multiple oscillation frequencies induced by finite width of the interferometer even with an STSB mode. The $h/2e$ AB oscillations, imposed by the Onsager relation in our closed-loop two-terminal geometry, appeared in the nodes of beats, while usual h/e AB oscillations appeared in the antinodes, which was in agreement with our simulation results. It was also found that nodes of the beats distributed parabolically with varying the voltages of the side gates. We confirm that the phenomena can be explained by the 2D multiple-longitudinal-modes effect in the presence of an STSB, even without resorting to the strong spin-orbit interaction.

*ycchung@pusan.ac.kr

†hjlee@postech.ac.kr

[1] Y. Aharonov and D. Bohm, Phys. Rev. **115**, 485 (1959).

[2] R. A. Webb, S. Washburn, C. P. Umbach, and R. B. Laibowitz, Phys. Rev. Lett. **54**, 2696 (1985).

[3] G. Timp, A. M. Chang, J. E. Cunningham, T. Y. Chang, P. Mankiewich, R. Behringer, and R. E. Howard, Phys. Rev. Lett. **58**, 2814 (1987).

[4] A. Yacoby, M. Heiblum, D. Mahalu, and Hadas Shtrikman, Phys. Rev. Lett. **74**, 4047 (1995).

[5] A. Yacoby, R. Schuster, and M. Heiblum, Phys. Rev. B **53**, 9583 (1996).

[6] R. Schuster, E. Buks, M. Heiblum, D. Mahalu, V. Umansky, and H. Shtrikman, Nature (London) **385**, 417 (1997).

[7] Yang Ji, M. Heiblum, D. Sprinzak, D. Mahalu, and Hadas Shtrikman, Science **290**, 779 (2000); Yang Ji, M. Heiblum, and Hadas Shtrikman, Phys. Rev. Lett. **88**, 076601 (2002); A. W. Holleitner, C. R. Decker, H. Qin, K. Eberl, and R. H. Blick, *ibid.* **87**, 256802 (2001).

[8] J. Liu, W. X. Gao, K. Ismail, K. Y. Lee, J. M. Hong, and S. Washburn, Phys. Rev. B **48**, 15148 (1993).

[9] W.-C. Tan and J. C. Inkson, Phys. Rev. B **53**, 6947 (1996).

[10] A. A. Bykov, Z. D. Kvon, and E. B. Ol'shanetskii, Proceedings of the 22nd International Symposium on Compound Semiconductors, 1996, pp. 909–914.

[11] A. F. Morpurgo, J. P. Heida, T. M. Klapwijk, B. J. van Wees, and G. Borghs, Phys. Rev. Lett. **80**, 1050 (1998).

[12] F. E. Meijer, A. F. Morpurgo, T. M. Klapwijk, J. Nitta, and T. Koga, Phys. Rev. B **69**, 035308 (2004).

[13] Jeng-Bang Yau, E. P. De Poortere, and M. Shayegan, Phys. Rev. Lett. **88**, 146801 (2002).

[14] M. J. Yang, C. H. Yang, and Y. B. Lyanda-Geller, Europhys. Lett. **66**, 826 (2004).

[15] M. V. Berry, Proc. R. Soc. London, Ser. A **392**, 45 (1984).

[16] U. Meirav, M. A. Kastner, and S. J. Wind, Phys. Rev. Lett. **65**, 771 (1990).

[17] G. Cernicchiaro, T. Martin, K. Hasselbach, D. Mailly, and A. Benoit, Phys. Rev. Lett. **79**, 273 (1997); S. Pedersen, A. E.

Hansen, A. Kristensen, C. B. Sørensen, and P. E. Lindelof, Phys. Rev. B **61**, 5457 (2000); R. Häussler, E. Scheer, H. B. Weber, and H. v. Löhneysen, *ibid.* **64**, 085404 (2001).

[18] A. D. Stone, Phys. Rev. Lett. **54**, 2692 (1985); S. Washburn and R. A. Webb, Rep. Prog. Phys. **55**, 1311 (1992).

[19] P. D. Dresselhaus, C. M. A. Papavassiliou, R. G. Wheeler, and R. N. Sacks, Phys. Rev. Lett. **68**, 106 (1992); C. Kurdak, A. M. Chang, A. Chin, and T. Y. Chang, Phys. Rev. B **46**, 6846 (1992).

[20] G. L. Chen, J. Han, T. T. Huang, S. Datta, and D. B. Janes, Phys. Rev. B **47**, 4084 (1993); S. Pedersen, C. B. Sørensen, A. Kristensen, P. E. Lindelof, L. E. Golub, and N. S. Averkiev, *ibid.* **60**, 4880 (1999); T. Koga, J. Nitta, T. Akazaki, and H. Takayanagi, Phys. Rev. Lett. **89**, 046801 (2002); J. B. Miller, D. M. Zumbühl, C. M. Marcus, Y. B. Lyanda-Geller, D. Goldhaber-Gordon, K. Campman, and A. C. Gossard, *ibid.* **90**, 076807 (2003).

[21] J. Luo, H. Munekata, F. F. Fang, and P. J. Stiles, Phys. Rev. B **38**, 10142 (1988); **41**, 7685 (1990); P. Ramvall, B. Kowalski, and P. Omling, *ibid.* **55**, 7160 (1997); W. Yang and K. Chang, *ibid.* **73**, 045303 (2006).

[22] J. Nitta, T. Akazaki, H. Takayanagi, and T. Enoki, Phys. Rev. Lett. **78**, 1335 (1997).

[23] M. Büttiker, Y. Imry, R. Landauer, and S. Pinhas, Phys. Rev. B **31**, 6207 (1985).

[24] S. K. Mitra, *Digital Signal Processing: A Computer-Based Approach* (McGraw-Hill, New York/Irwin, Boston, 2001).

[25] A. V. Oppenheim, R. W. Schafer, and J. R. Buck, *Discrete-Time Signal Processing* (Prentice-Hall, Upper Saddle River, NJ, 1999).

[26] Apoorva G. Wagh and Veer Chand Rakhecha, Phys. Rev. Lett. **90**, 119703 (2003).

[27] A. G. Mal'shukov and K. A. Chao, Phys. Rev. Lett. **90**, 179701 (2003).

[28] In our measurements, we first checked separately that the paths between each of the six gates (side gates 1, 2, 3, and 4 and quantum-dot gates 1 and 2 in Fig. 1) and the island gate (in Fig. 1) gave a single transverse subband mode by tuning each corresponding conductance below $2e^2/h$. We then checked the conductance through the interferometer as a whole to be lower than $2e^2/h$. This confirmed us that the interferometer kept only a single transverse subband mode. The resulting conductance with the subtraction of the background revealed clear AB oscillations with beats even for a low visibility.